Sb$_2$S$_3$ with Various Nanostructures: Controllable Synthesis, Formation Mechanism, and Electrochemical Performance toward Lithium Storage

Jianmin Ma, Xiaochuan Duan, Jiabiao Lian, Tongil Kim, Peng Peng, Xiaodi Liu, Zhifang Liu, Haobo Li, and Wenjun Zheng*[a]

Abstract: The size- and shape-controlled synthesis of Sb$_2$S$_3$ nanostructures has been successfully realized by a facile hydrothermal route. A range of dimensional nanostructures, such as one-dimensional nanorods, two-dimensional nanowire bundles, three dimensional sheaf-like superstructures, dumbbell-shaped superstructures, and urchin-like microspheres, could be obtained through introducing different organic complex reagents or ionic liquids to the reaction system. The formation mechanisms of various Sb$_2$S$_3$ nanostructures have been rationally proposed based on the crystal structure and the nature of the complex reagents and the ionic liquid. The effects of experimental parameters on the final product are also discussed in detail. In addition, electrochemical measurements demonstrate that the as-synthesized Sb$_2$S$_3$ nanostructures have higher initial Li intercalation capacity and excellent cyclic performances, which indicates that the as-synthesized Sb$_2$S$_3$ nanostructures could have potential applications in commercial batteries.

Keywords: antimony · crystal growth · ionic liquids · nanostructures · self-assembly

Introduction

During the last decade, one-dimensional (1D) nanostructures, such as nanorods, nanotubes, and nanowires, have been of great interest due to their size- and geometry-dependent properties[1] and widespread potential applications.[2] So far, intensive efforts have been devoted to developing numerous 1D nanostructures through various techniques and methods.[3] Currently, the organization and manipulation of these 1D nanostructures are intensively investigated to advance the science and technology of the application of 1D nanostructures in functional nanodevices, which depend strongly on the ability to assemble ordered and complex architectures.[4] These complex architectures open up possibilities for advanced nanodevices.[5] Their collective behavior and interparticle coupling in well-organized 1D nanostructures would result in new functions or significant improvement in the optoelectronic properties.[6] Various procedures, including the Langmuir–Blodgett technique,[7] biorecognition,[8] microfluidic,[9] nanoimprinting,[10] template-directed self-organization,[11] and external electric- or magnetic-field-induced alignment,[4, 12] have been developed to assemble 1D nanomaterials into ordered patterns. However, rationally manipulating the morphology and architecture of inorganic materials in solution remains a challenge for material design.

Room-temperature ionic liquids (RTILs) have been successfully used in various fields[13] due to their unique properties: a large electrochemical window, polar but with low interface tension, low interface energies, high thermal stability, and extended hydrogen-bond systems. Recently, RTILs have received increasing attention from the inorganic materials community because they can produce inorganic materials with new structures and properties.[14] To date, many RTIL-involved processes, including electrodeposition,[15] photochemical reduction,[16] electron beam irradiation,[17] sol-gel processes,[18] and solvothermal[19] and ionothermal routes,[20] have been developed to synthesize inorganic nanomaterials. RTILs have been proved to be excellent media for inorganic synthesis and could offer many opportunities and challenges for the synthesis of unique structured nanoparticles. However, this new type of reaction medium needs to be further explored for other inorganic systems. Therefore, we have attempted to control the growth of various Sb$_2$S$_3$ nanostruc-

[a] Dr. J. Ma, Dr. X. Duan, Dr. J. Lian, Dr. T. Kim, Dr. P. Peng, Dr. X. Liu, Z. Liu, H. Li, Prof. W. Zheng
Department of Materials Chemistry and Key Laboratory of Advanced Energy Materials Chemistry (MOE)
College of Chemistry, Nankai University
Tianjin, 300071 (P. R. China)
Fax: (+66) 022-23502604
E-mail: zhwj@nankai.edu.cn

Supporting information for this article is available on the WWW under http://dx.doi.org/10.1002/chem.201000962.

tures under hydrothermal conditions with a combination of ionic liquid and other additives.

As a known layer-structured semiconductor with a direct band gap of 1.78 eV, Sb_2S_3 has many potential applications, including solar energy conversion,[21] thermoelectric cooling technologies, and optoelectronics in the IR region.[22] Recently, Sun et al.[23] found that Sb_2S_3 exhibited efficient photocatalytic properties in the decomposition of methyl orange and *p*-hydroxyazobenzene. Because of these useful properties, considerable efforts have been devoted to the fabrication of Sb_2S_3 films and controlled synthesis of 1D Sb_2S_3 nanostructures, as well as more complex assemblies. Various Sb_2S_3 films have been fabricated by different methods, such as chemical bath deposition,[24] thermal evaporation,[25] and spray pyrolysis techniques.[26]. Simple 1D Sb_2S_3 nanostructures, including nanorods,[27] nanowires,[28] nanotubes,[29] and nanoribbons,[30] have been produced by various synthetic routes. Moreover, complex Sb_2S_3 superstructures including hollow ovoid microcrystals,[31] sheaf-like superstructures,[32] nanorod-bundles,[33] and straw-tied-like architectures,[34] have been obtained in solution. However, most methods employed toxic reagents or used a polymer as a template. Therefore, it is highly desirable to explore a simple, polymer-free, environmentally friendly route to fabricate complex Sb_2S_3 superstructures and controllable 1D nanostructures.

Recent studies demonstrate that some minerals in nature tend to form unusual morphologies by crystal splitting during their growth. With knowledge of crystal growth kinetics, crystal splitting can be adjusted to fabricate novel morphologies. Splitting ability in minerals strongly depends on their crystal structure. A range of materials, such as sheaf-like Bi_2S_3 and β-FeO(OH),[35] sheaf-like hierarchical Sb_2S_3 and Sb_2Se_3,[32] and sheaf-like $BaWO_4$ with different degrees of crystal splitting,[36] bundle-like, cross-like and spherulitic Fe_2P,[37] have been fabricated by crystal splitting processes. On the other hand, self-assembly is considered to be an effective strategy to form hierarchical superstructures. Self-assembly of nanocrystals is usually driven by van der Waals forces and hydrogen bonding between certain organic molecules on the particle surface.[38] Thus, it is desirable to develop an effective synthetic approach to delicately control the growth of Sb_2S_3 nanostructures by a combination of crystal splitting and self-assembly techniques.

Herein, we report morphology manipulation of Sb_2S_3 nanocrystals under hydrothermal condition with different additives in the synthetic system. Furthermore, the formation mechanisms of various Sb_2S_3 nanostructures were discussed in detail from the viewpoints of crystal growth habit and the effects of the ionic liquid and other additives. Moreover, electrochemical measurements demonstrate that the as-synthesized Sb_2S_3 nanostructures display a higher initial Li intercalation capacity and excellent cyclic performances.

Results and Discussion

The morphology and size of the as-synthesized products were characterized by scanning electron microscopy (SEM) and transmission electron microscopy (TEM). Figure 1a–d
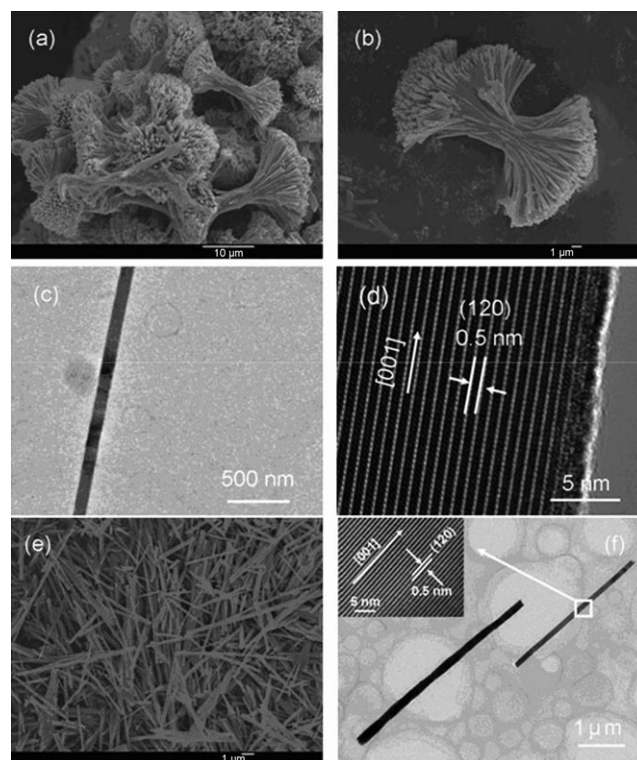

Figure 1. a) Low-magnification and b) high-magnification SEM images of the as-prepared sheaf-like Sb_2S_3 superstructures. c) TEM image and d) HRTEM image of an individual nanorod from the sheaf-like Sb_2S_3 superstructures. e) SEM image and f) TEM image of the as-prepared Sb_2S_3 nanorods; inset: HRTEM image. Scale bars: a) 10 μm, b) 1 μm, e) 1 μm.

shows the product synthesized with ionic liquid [Bmim]Cl (4 mol L^{-1}) and citric acid (0.04 mol L^{-1}) at 180 °C for 5 h. Self-assembled Sb_2S_3 products with an average horizontal axis of around 2.5 μm and a longitudinal axis of around 20 μm on a large scale were observed (Figure 1a). The high-resolution SEM image (Figure 1b) reveals an individual Sb_2S_3 microparticle consisting of aligned nanorods with diameters of about 50 nm. Furthermore, we also investigated nanorods arranged side-by-side in an ordered fashion. The detailed structure of the as-prepared sheaf-like nanostructures has further been studied by TEM analysis (Figure 1c and d). Figure 1c displays a low-magnification image of a single nanorod with a diameter of about 50 nm. And the corresponding high-resolution TEM (HRTEM) image of the nanorod (Figure 1d) exhibits good crystalline and clear lattice fringes. The interlayer distance is found to be 0.5 nm, which corresponds to the (120) plane of Sb_2S_3. The lattice planes are well aligned in a parallel manner without any notable defects, which is important for optoelectronic applications. The Sb_2S_3 nanorods in Figure 1e and f were synthe-

sized with ammonium citrate (0.04 mol L^{-1}) in the absence of ionic liquid at 180 °C for 24 h. SEM images of the product indicate rod-like morphology with a diameter of 100 to 150 nm and several micrometers in length (Figure 1e). The sample was further characterized by TEM and HRTEM (Figure 1f) to obtain more information on the structure and morphology. HRTEM image of the circled part of the nanorod (Figure 1f, inset) indicates good crystalline and clear lattice fringes. It reveals that the lattice-resolved fringes with a constant spacing of 0.5 nm, which correspond to the (120) planes, are parallel to the nanorod axis. Thus, it can be inferred that the growth direction of the nanorod is along the [001] direction.

The phase and purity of the as-obtained products were examined by X-ray diffraction (XRD). The XRD patterns of the as-prepared sheaf-like Sb$_2$S$_3$ nanostructures and nanorods are shown in Figure 2a and b, respectively. All the dif-
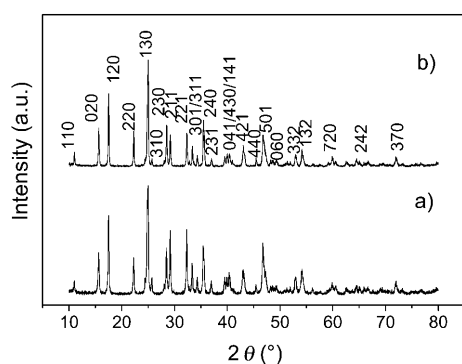

Figure 2. XRD patterns of the as-synthesized Sb$_2$S$_3$ nanostructures: a) sheaf-like nanostructures and b) nanorods.

fraction peaks can be readily indexed to orthorhombic Sb$_2$S$_3$ (JCPDS Card No. 06-0474); no peaks from other phases were observed, which indicates the high purity of the products. It is also observed that all the major (hk0) planes are of relatively higher intensity compared with their reported value. This indicates that the preferential crystal growth is along the (00l) direction, in agreement with the one-dimensional growth of the materials. This phenomenon may be caused by preferential growth along the (120) plane and a closely packed and ordered structure.

In general, the final shape of nanocrystals was controlled by the inherent crystal structure during the initial nucleation stage and subsequent growth stage through the delicate control of external factors, such as the additive, reaction media, and reaction time.[39] Therefore, the final crystalline morphology is the cooperative result of internal crystal factors and external controlled factors.

A typical Sb$_2$S$_3$ crystal structure (Figure 3) consists of infinite chains of (Sb$_4$S$_6$)$_n$ moieties running parallel to the c-axis and close to the [010] directions that contain two types of Sb and three types of S atoms.[40] Two sulfur atoms are formally trivalent and one is divalent. Within the chain, the divalent sulfur and one of the trivalent sulfurs are connected
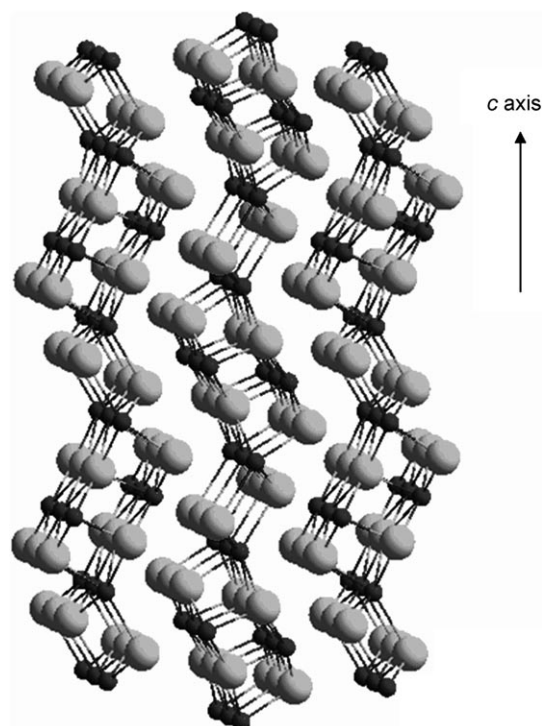

Figure 3. Schematic illustration of the crystal structure of Sb$_2$S$_3$. Dark grey spheres represent Sb, light grey spheres represent S.

to antimony by strong covalent bonds. However, the third sulfur is connected to the antimony of the second parallel running chain by weaker van der Waals bonds, which are responsible for the cleavage of the crystal. Thus, the cleavage occurs parallel to the (010) planes, in which only van der Waals bonds are ruptured. Consequently, Sb$_2$S$_3$ breaks easily along the c-axis and leads to the formation of 1D nanostructures and complex nanorod structures. In addition, the morphology evolution processes (Figure S1 in the Supporting Information) support the fractal splitting growth mechanism for the sheaf-like nanostructures. Also, it has been shown that the complex structures of the nanorods indeed grow along the [001] direction based on our HRTEM measurements, which provides additional support for the fractal splitting growth mechanism.

The ability to assemble nanoscopic components into larger structures depends crucially on the interparticle interactions. In a solution-phase synthesis, the specific molecular interactions between capping agents can contribute to significant and specific interparticle potentials between much larger components and enable their spontaneous organization into a variety of ordered structures.[41] To manipulate the morphology of Sb$_2$S$_3$ nanocrystals, we introduced citrate acid and ammonium citrate separately into this solvothermal synthesis. It is believed that there are COOH and OH functional groups on the citric acid, which has a strong tendency to coordinate with inorganic metal cations, such as Ag$^+$, Ca^{2+}, Mg^{2+}, Ni^{2+}, and Zn^{2+}.[42] The presence of these groups has made citric acid a useful self-assembly reagent in our system. It is known that self-assembly of nanocrystals is

driven by van der Waals forces and hydrogen bonding among certain organic molecules on the particle surface. At the nanoscale, hydrogen bonding has been shown to initiate the aggregation of nanoparticles functionalized with hydrogen-bonding ligands, in which the degree of aggregation and ordering depends on the strength of individual hydrogen bonds. When these groups are carboxylic, the interactions depend on the pH of the surrounding solution and exhibit strong hydrogen-bond interactions at low pH and repulsive electrostatic interactions at high pH.[41,43] In this way, the balance between hydrogen-bond attraction and electrostatic repulsion gives way to side-to-side assemblies governed predominantly by van der Waals forces. Thus, irregular sheaf-like Sb$_2$S$_3$ hierarchical nanostructures (Figure S2 in the Supporting Information) could be obtained if citric acid was used as self-assembly reagent. By introducing a proper amount of ionic liquid [Bmim]Cl to the present system, the well-defined sheaf-like Sb$_2$S$_3$ superstructures (Figure 1a) could be obtained. Though [Bmim]Cl slowed down the reaction, its good dispersancy and high viscosity made the products smaller and more regular as they grew gradually because the mass transport was hindered. On the other hand, the pH of solution was enhanced when an equimolar amount of ammonium citrate replaced citrate acid in the reaction system. The change in pH breaks the balance between the hydrogen-bond interactions and repulsive electrostatic interactions of Sb$_2$S$_3$ nanorods in the presence of citrate anions, then lowers the interparticle interaction and further leads to the formation of nanorods rather than sheaf-like nanostructures. In addition, if ammonium citrate was not used while keeping the other conditions the same as those of Sb$_2$S$_3$ nanorods, irregular microrods were obtained (Figure S3 in the Supporting Information). These results indicate that additives are important for the formation of the Sb$_2$S$_3$ nanostructures during the solvothermal process. Schematic illustrations of the interactions between the Sb$_2$S$_3$ surfaces in the presence of citric acid and ammonium citrate are shown in Figure 4a and b, respectively.
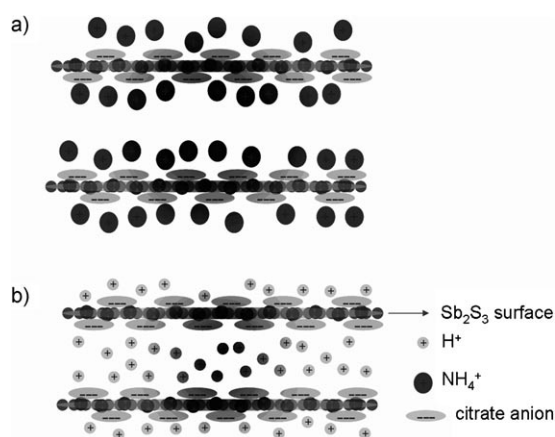

Figure 4. Schematic illustration of the interactions between the Sb$_2$S$_3$ surfaces in the presence of different additives: a) citric acid and b) ammonium citrate.

Our synthetic parameters enable further shape manipulation of Sb$_2$S$_3$ hierarchical architectures. The concentration of citric acid can significantly affect the shape of the products. With a citric acid concentration of 0.02 mol L^{-1}, without any ionic liquid, and with the other reaction conditions kept the same, the Sb$_2$S$_3$ hierarchical architectures (Figure 5a) mainly
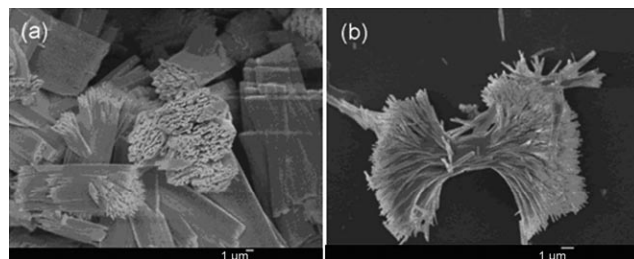

Figure 5. SEM images of Sb$_2$S$_3$ samples obtained under various synthetic conditions: a) citric acid (0.02 mol L^{-1}), no ionic liquid, and the other experimental parameters were kept the same as for the sheaf-like Sb$_2$S$_3$ superstructures; b) citric acid (0.02 mol L^{-1}), ionic liquid (4 mol L^{-1}), and the other experimental parameters were kept the same as for the sheaf-like Sb$_2$S$_3$ superstructures. Scale bars: a) 1 μm, b) 1 μm.

consists of unique column-like superstructures of ≈5 μm diameter. If the concentration of citric acid was increased to 0.06 mol L^{-1}, urchin-like microspheres and many nanorods (Figure S3 in the Supporting Information) were obtained. Moreover, the ionic liquid also played a crucial role in manipulating the morphology of final product. Dumbbell-shaped Sb$_2$S$_3$ superstructures (Figure 5b), similar to sheaf-like superstructures, could be obtained if a proper concentration of ionic liquid (4 mol L^{-1}) was used in the presence of citric acid (0.02 mol L^{-1}). The two SEM images (Figure 5) indicate that the ionic liquid strongly influenced the morphology of the final product and favored the cleavage of the superstructures under these conditions. The splitting process of the dumbbell-shaped superstructures is given in Figure S5 in the Supporting Information. In a divergence from the roles of ionic liquid in the discussion above, a steric hindrance effect of the imidazolium cations of the ionic liquid between the surfaces of Sb$_2$S$_3$ nanorods was suggested to contribute to the formation of the sheaf-like superstructures. The steric hindrance effect partly offsets the hydrogen-bond interactions and the van der Waals bonds between the parallel running chains, and contributes to the cleavage parallel to the (010) planes and subsequently the formation of the dumbbell-shaped superstructures. A schematic illustration of the interactions between the Sb$_2$S$_3$ surfaces in the presence of citric acid and [Bmim]Cl is given in Figure 6a.

As demonstrated above, the ionic liquid indeed plays crucial roles in controlling the growth and self-assembly of Sb$_2$S$_3$ nanostructures. To investigate the influence of the concentration of ionic liquid on the morphology of final products in the aqueous ammonium citrate system, two control experiments were carried out by adjusting the concentration of [Bmim]Cl while other conditions remained unchanged. When a low concentration of ionic liquid (0.8 mol L^{-1}) was
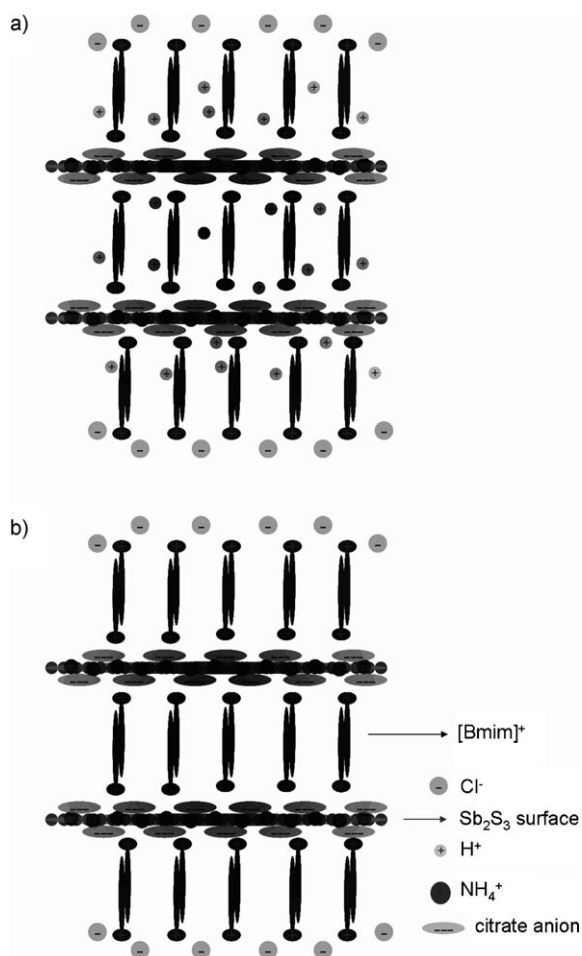
Figure 6. Schematic illustration of the interactions between the Sb$_2$S$_3$ surfaces in the presence of [Bmim]Cl and a) citrate acid or b) ammonium citrate.

introduced into the reaction system, some Sb$_2$S$_3$ nanorod bundles (Figure 7a) could be obtained. When a high concentration of ionic liquid (4 mol L^{-1}) was used, urchin-like Sb$_2$S$_3$ microspheres (Figure 7b) could be obtained. To evaluate detailed roles in the nanorods bundles and urchin-like micro-
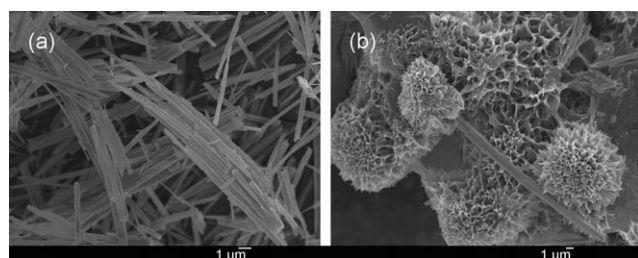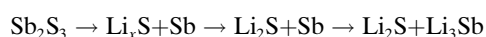

Figure 7. SEM images of Sb$_2$S$_3$ samples obtained under various synthetic conditions: a) ammonium citrate (0.04 mol L^{-1}), ionic liquid (0.8 mol L^{-1}), and the other experimental parameters were kept the same as for the sheaf-like Sb$_2$S$_3$ superstructures; b) ammonium citrate (0.04 mol L^{-1}), ionic liquid (4 mol L^{-1}), and the other experimental parameters were kept the same as for the dumbbell-shaped Sb$_2$S$_3$ superstructures. Scale bars: a) 1μm, b) 1 μm.

spheres of Sb$_2$S$_3$, their morphology evolution processing experiments were conducted (Figure S6 and 7 in the Supporting Information). Based on the experimental results, we think that the roles of the ionic liquid should be emphasized. The self-assembly effect of ionic liquid can be attributed to a combination of the van der Waals forces between the ionic liquid molecules and the hydrogen-bond interactions and electrostatic forces between the citrate cations and ionic liquid. It is recognized that the imidazolium-based ionic liquid has a polymeric supramolecular structure composed of anionic and cationic aggregates, along with the extraordinary potential to generate a nanostructure with polar and nonpolar regions in which the nanoparticles are embedded.[14,44] [Bmim]Cl is considered to form a protective layer surrounding the nanoparticles, which is composed of semiorganized imidazolium cationic supramolecular aggregates located immediately adjacent to the nanoparticle surface. This provides stabilization whereas counterions provide charge balance, which is close to Darjaugin–Landau–Verwey–Overbeek-type stabilization.[44,45] Electrostatic interaction provided by the intrinsic high charge of [Bmim]Cl and steric hindrance due to the supramolecular anionic and cationic aggregates adjusts the interaction between Sb$_2$S$_3$ nanorods; consequently, the complete coating of supramolecular aggregates of [Bmim]Cl on Sb$_2$S$_3$ nanorods keeps them well spaced from each other. On the other hand, these interactions cause the nanorods in the superstructures to bind together and thus inhibit the cleavage to form the superstructures. A schematic illustration of the interactions between the Sb$_2$S$_3$ surfaces in the presence of ammonium citrate and [Bmim]Cl is shown in Figure 6b. On the other hand, the initial nucleation and subsequent growth of Sb$_2$S$_3$ nanocrystals, which strongly depend on the reaction parameters, particularly the reaction media, lead to the formation of different morphologies. Considering the complicated properties of ionic liquid, the detailed roles of ionic liquid need further investigation.

To investigate the morphology-dependent of the electrochemical properties of the three Sb$_2$S$_3$ nanostructures, we carried out a preliminary assessment of their electrochemical performance with respect to Li insertion/extraction. Figure 8 shows the first discharge/charge voltage profiles for the Sb$_2$S$_3$ column-like superstructures, nanorods, and sheaf-like superstructures at a current density of 50 mA g^{-1} in the voltage window of 0.01 to 3.0 V (vs. Li$^+$/Li). The shape of the three curves is very similar, indicating that the morphology and size do not change the lithium storage nature of Sb$_2$S$_3$. During the first discharge process, two discharge plateaus at 1.45 and 0.65 V (Figure 8) were observed and provided an initial capacity of 1074, 1175, and 1154 mAh g^{-1} for column-like superstructures, nanorods, and sheaf-like superstructures, respectively. Sohn et al.[46] reported that the electrochemical reaction occurring in the Sb$_2$S$_3$ electrode is as follows:
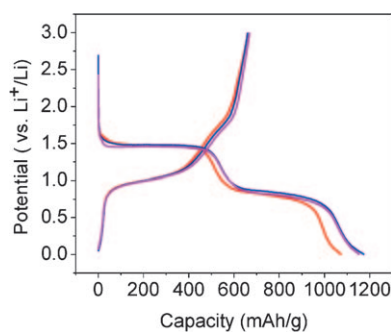
$$Sb_2S_3 \rightarrow Li_xS + Sb \rightarrow Li_2S + Sb \rightarrow Li_2S + Li_3Sb$$

FULL PAPER

Figure 8. Electrochemical Li intercalation/deintercalation curves of Sb$_2$S$_3$ samples: ——: column-like superstructures, ——: nanorods, and ——: sheaf-like superstructures.

Figure 9 shows the discharge capacity versus cycle number for electrodes made from the column-like superstructures, nanorods, and sheaf-like superstructures of Sb$_2$S$_3$ at a cur-
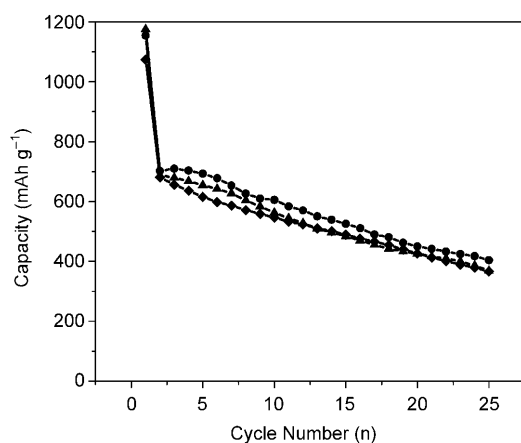

Figure 9. The discharge capacities of Sb$_2$S$_3$ samples as a function of cycle number: ◆: column-like superstructures, ▲: nanorods, and ●: sheaf-like superstructures.

rent density of 50 mA g^{-1}, respectively. After 25 cycles, the reversible capacity for sheaf-like superstructures is still as high as 425 mAh g^{-1}, whereas that for column-like superstructures and nanorods is only 367 and 377 mAh g^{-1}, respectively. The sheaf-like Sb$_2$S$_3$ superstructures are superior to the other samples, with the highest lithium storage capacity, lowest irreversible loss, and excellent cycling performance, which may be attributed to its special structure and smaller size of nanorods.[47] The sheaf-like Sb$_2$S$_3$ superstructures are composed of nanorods with a relatively smaller diameter; this special structure favors both the diffusion of the lithium ion and the electrolyte and Sb$_2$S$_3$. Therefore, better electrochemical property is observed for the sheaf-like Sb$_2$S$_3$ superstructures. In addition, their Li intercalation/deintercalation reversibility is better than the values reported for In$_2$S$_3$, Bi$_2$S$_3$, and pure Sb$_2$S$_3$ nanostructures.[46,48] These results indicate that synthetic Sb$_2$S$_3$ nanostructures can be potentially applied to be anode material for lithium ion batteries.

Conclusion

In summary, we have developed a facile hydrothermal method for the controllable synthesis of Sb$_2$S$_3$ nanostructures with a range of sizes and morphologies. Sb$_2$S$_3$ with various dimensional nanostructures, such as 1D nanorods, 2D nanowire bundles, 3D sheaf-like superstructures, dumbbell-shaped superstructures, and urchin-like microspheres, could be obtained by properly monitoring the experimental conditions, such as the concentration of complex reagent, different complex reagent, and ionic liquid. On the basis of the observation of intermediate products in the growth process, the formation mechanisms of various Sb$_2$S$_3$ nanostructures are proposed. Moreover, the as-synthesized Sb$_2$S$_3$ nanostructures showed higher initial Li intercalation capacity over graphite anode materials and excellent cyclic performances. The present work opens new strategies for the controllable synthesis of various nanostructures from 1D to 3D nanoscale building blocks, and provides a step forward in the design of novel anode materials with higher electrochemical capacity.

Experimental Section

Chemicals: All chemicals were of analytical grade and were used without further purification. The ionic liquid 1-*n*-butyl-3-methylimidazolium chloride ([bmim]Cl) was prepared according to the literature.[49]

Synthesis: In a typical synthesis of Sb$_2$S$_3$ nanostructures, Sb(CH$_3$COO)$_3$ (1 mmol) and a given concentration of additive (citric acid or ammonium citrate) were added to a mixture of distilled water and ionic liquid [Bmim]Cl (25 mL) and stirred vigorously. Then, a given amount of thioacetamide (TAA) was added to the solution and the mixture was transferred into an autoclave and maintained at a fixed temperature for a predetermined time, then allowed to cool to RT. Finally, the black precipitate was collected and washed three times with absolute ethanol and water.

Characterization: XRD analysis was performed by using a Rigaku D/max Diffraction System with a Cu$_{Kα}$ source ($λ = 0.15406$ nm). The SEM images were taken by using a JEOLJSM-6700F field-emission scanning electron microscope (15 kV). The TEM images were taken by using a Hitachi model H-800 transmission electron microscope with an accelerating voltage of 200 kV. HRTEM photographs were obtained by using a JEOL-2010 transmission electron microscope.

Electrochemical measurements: The electrochemical Li intercalation performance was investigated in Li test cells for Sb$_2$S$_3$ samples with various morphologies. The Sb$_2$S$_3$ sample was mixed with acetylene black and polytetrafluoroethylene with a weight ratio of 75:15:10 in ethanol to ensure homogeneity. After the ethanol was evaporated, the mixture was rolled into a sheet and cut into circular strips of 8 mm diameter. The strips were then dried at 120 °C for 10 h in air. Lithium metal was used as the counter and reference electrodes. The electrolyte was composed of a solution of LiPF$_6$ (1 M) in ethylene carbonate/dimethyl carbonate with a weight ratio of 1:1. These parts were assembled into test cells in an argon-filled dry glovebox, and then the cells were measured at a current density of 60 mA g^{-1} within a voltage range of 0.01–3.0 V by using a Land CT2001 battery tester.

Acknowledgements

[1] a) H. Dai, J. H. Hafner, A. G. Rinzler, D. T. Colbert, R. E. Smalley, *Nature* **1996**, *384*, 147–150; b) X. G. Peng, L. Manna, W. D. Yang, J. Wickham, E. Scher, A. Kadavanich, A. P. Alivisatos, *Nature* **2000**, *404*, 59–61; c) Y. N. Xia, P. D. Yang, Y. G. Sun, Y. Y. Wu, B. Mayers, B. Gates, Y. D. Yin, F. Kim, H. Q. Yan, *Adv. Mater.* **2003**, *15*, 353–389; d) P. K. Jain, S. Eustis, M. A. El-Sayed, *J. Phys. Chem. B* **2006**, *110*, 18243–18253; e) J. M. Ma, Y. P. Wang, Y. J. Wang, Q. Chen, J. B. Lian, W. J. Zheng, *J. Phys. Chem. C* **2009**, *113*, 13588–13592.

[2] a) D. S. Xu, Y. J. Xu, D. P. Chen, G. L. Guo, L. L. Gui, Y. Q. Tang, *Adv. Mater.* **2000**, *12*, 520–522; b) Z. W. Pan, Z. R. Dai, Z. L. Wang, *Science* **2001**, *291*, 1947–1949; c) C. H. Liu, J. A. Zapien, Y. Yao, X. M. Meng, C. S. Lee, S. S. Fan, Y. Lifsitz, S. T. Lee, *Adv. Mater.* **2003**, *15*, 838–841; d) J. Zhou, Y. Ding, S. Z. Deng, L. Gong, N. X. Xu, Z. L. Wang, *Adv. Mater.* **2005**, *17*, 2107–2110; e) B. S. Guiton, Q. Gu, A. L. Prieto, M. S. Gudiksen, H. Park, *J. Am. Chem. Soc.* **2005**, *127*, 498–499; f) L. Ouyang, E. S. Thrall, M. M. Deshmukh, H. Park, *Adv. Mater.* **2006**, *18*, 1437–1440.

[3] a) X. Duan, C. M. Lieber, *Adv. Mater.* **2000**, *12*, 298–302; b) Y. J. Zhu, W. W. Wang, R. J. Qi, X. L. Hu, *Angew. Chem.* **2004**, *116*, 1434–1438; *Angew. Chem. Int. Ed.* **2004**, *43*, 1410–1424; c) J. W. Grebinski, K. L. Richter, J. Zhang, T. H. Kosel, M. Kuno, *J. Phys. Chem. B* **2004**, *108*, 9745–9751; d) R. Adelung, O. C. Aktas, J. Franc, A. Biswas, R. Kunz, M. Elbahri, J. Kanzow, U. Schuermann, F. Faupel, *Nat. Mater.* **2004**, *3*, 375–379; e) C. Ma, Z. L. Wang, *Adv. Mater.* **2005**, *17*, 2635–2639; f) S. Milenkovic, A. W. Hassel, A. Schneider, *Nano Lett.* **2006**, *6*, 794–799.

[4] J. Y. Yuan, H. T. Gao, F. Schacher, Y. Y. Xu, R. Richter, W. Tremel, A. H. E. Müller, *ACS Nano* **2009**, *3*, 1441–1450.

[5] a) R. C. Jin, Y. W. Cao, C. A. Mirkin, K. L. Kelly, G. C. Schatz, J. G. Zheng, *Science* **2001**, *294*, 1901–1903; b) Y. Huang, X. F. Duan, C. M. Lieber, *Small* **2005**, *1*, 142–147.

[6] a) L. S. Li, J. Walda, L. Manna, A. P. Alivisatos, *Nano Lett.* **2002**, *2*, 557–560; b) Y. F. Zhu, M. Chen, Z. Wei, R. P. Zhang, K. Nikhil, L. Ji, *J. Appl. Phys.* **2009**, *105*, 0543191.

[7] a) F. Kim, S. Kwan, J. Akana, P. D. Yang, *J. Am. Chem. Soc.* **2001**, *123*, 4360–4361; b) S. Acharya, J. P. Hill, K. Ariga, *Adv. Mater.* **2009**, *21*, 2959–2964; c) L. Q. Mai, Y. H. Gu, C. H. Han, B. Hu, W. Chen, P. C. Zhang, L. Xu, W. L. Guo, Y. Dai, *Nano Lett.* **2009**, *9*, 826–830.

[8] a) K. K. Caswell, J. N. Wilson, U. H. F. Bunz, C. J. Murphy, *J. Am. Chem. Soc.* **2003**, *125*, 13914–13915; b) M. Sethi, G. Joung, M. R. Knecht, *Langmuir* **2009**, *25*, 1572–1581.

[9] a) Y. Huang, X. F. Duan, Q. Q. Wei, C. M. Lieber, *Science* **2001**, *291*, 630–633; b) K. Oh, J. H. Chung, J. J. Riley, Y. L. Liu, W. K. Liu, *Langmuir* **2007**, *23*, 11932–11940; c) S. E. Chung, W. Park, S. Shin, S. A. Lee, S. Kwon, *Nat. Mater.* **2008**, *7*, 581–587.

[10] N. A. Melosh, A. Boukai, F. Diana, B. Gerardot, A. Badolato, P. M. Petroff, J. R. Heath, *Science* **2003**, *300*, 112–114.

[11] a) M. A. Correa-Duarte, J. Perez-Juste, A. Sanchez-Iglesias, M. Giersig, L. M. Liz-Marzan, *Angew. Chem.* **2005**, *117*, 4449–4452; *Angew. Chem. Int. Ed.* **2005**, *44*, 4375–4378; b) Q. Zhang, S. Gupta, T. Emrick, T. P. Russell, *J. Am. Chem. Soc.* **2006**, *128*, 3898–3899; c) T. Li, L. Y. Wu, N. Suthiwangcharoen, M. A. Bruckman, D. Cash, J. S. Hudson, S. Ghoshroy, Q. Wang, *Chem. Commun.* **2009**, 2869–2871.

[12] a) C. M. Hangarter, N. V. Myung, *Chem. Mater.* **2005**, *17*, 1320–1324; b) S. Gupta, Q. Zhang, T. Emrick, T. P. Russell, *Nano Lett.* **2006**, *6*, 2066–2069; c) K. M. Ryan, A. Mastroianni, K. A. Stancil, H. Liu, A. P. Alivisatos, *Nano Lett.* **2006**, *6*, 1479–1482; d) C. M. Hangarter, Y. Rheem, B. Yoo, E. H. Yang, N. V. Myung, *Nanotechnology* **2007**, *18*, 205305/1–7.

[13] a) L. A. Blanchard, D. Hancu, E. J. Beckman, J. E. Brennecke, *Nature* **1999**, *399*, 28–29; b) F. Endres, M. Bukowski, H. Hempelmann, H. Natter, *Angew. Chem.* **2003**, *115*, 3550–3552; *Angew.*

[13] *Chem. Int. Ed.* **2003**, *42*, 3428–3430; c) N. Jain, A. Kumar, S. M. S. Chauhan, *Tetrahedron* **2005**, *61*, 1015–1060.

[14] M. Antonietti, D. Kuang, B. Smarsly, Y. Zhou, *Angew. Chem.* **2004**, *116*, 5096–5100; *Angew. Chem. Int. Ed.* **2004**, *43*, 4988–4992.

[15] a) I. Mukhopadhyay, W. Freyland, *Langmuir* **2003**, *19*, 1951–1953; b) O. Mann, W. Freyland, O. Raz, Y. Ein-Eli, *Chem. Phys. Lett.* **2008**, *460*, 178–181; c) R. Bomparola, S. Caporali, A. Lavacchi, U. Bardi, *Surf. Coat. Technol.* **2007**, *201*, 9485–9490; d) Y. Bando, Y. Katayama, T. Miura, *Electrochim. Acta* **2007**, *53*, 87–91.

[16] a) J. M. Zhu, Y. H. Shen, A. J. Xie, L. G. Qiu, Q. Zhang, S. Y. Zhang, *J. Phys. Chem. C* **2007**, *111*, 7629–7633; b) C. Zhao, A. M. Bond, *J. Am. Chem. Soc.* **2009**, *131*, 4279–4287.

[17] A. Imanishi, M. Tamura, S. Kuwabata, *Chem. Commun.* **2009**, 1775–1777.

[18] a) H. F. Wang, Y. Z. Zhu, X. P. Yan, R. Y. Gao, J. Y. Zheng, *Adv. Mater.* **2008**, *20*, 952–954; b) H. Farag, M. Al Zoubi, F. Endres, *J. Mater. Sci.* **2009**, *44*, 122–128; c) Y. Zhou, M. Antonietti, *J. Am. Chem. Soc.* **2003**, *125*, 14960–14961.

[19] a) W. S. Dong, F. Q. Lin, C. L. Liu, M. Y. Li, *J. Colloid Interface Sci.* **2009**, *333*, 734–740; b) J. B. Lian, X. C. Duan, J. M. Ma, T. I. Kim, W. J. Zheng, *ACS Nano* **2009**, *3*, 3749–3761; c) X. D. Liu, J. M. Ma, P. Peng, W. J. Zheng, *Langmuir* **2010**, *26*, 9968–9973; d) J. M. Ma, L. Chang, J. B. Lian, Z. Huang, X. C. Duan, X. D. Liu, P. Peng, T. I. Kim, Z. F. Liu, W. J. Zheng, *Chem. Commun.* **2010**, *46*, 5006–5008.

[20] a) E. R. Cooper, C. D. Andrews, P. S. Wheatley, P. B. Webb, P. Wormald, R. E. Morris, *Nature* **2004**, *430*, 1012–1016; b) J. B. Lian, T. I. Kim, X. D. Liu, J. M. Ma, W. J. Zheng, *J. Phys. Chem. C* **2009**, *113*, 9135–9140; c) Z. J. Lin, D. S. Wragg, R. E. Morris, *Chem. Commun.* **2006**, 2021–2033; d) H. G. Zhu, J. F. Huang, Z. W. Pan, S. Dai, *Chem. Mater.* **2006**, *18*, 4473–4477; e) N. Recham, L. Dupont, M. Courty, K. Djellab, D. Larcher, M. Armand, J. M. Tarascon, *Chem. Mater.* **2009**, *21*, 1096–1107.

[21] a) O. Savadogo, K. C. Mandal, *Sol. Energy Mater. Sol. Cells* **1992**, *26*, 117–136; b) Y. Itzhaik, O. Niitsoo, M. Page, G. Hodes, *J. Phys. Chem. C* **2009**, *113*, 4254–4256.

[22] D. Arivuoli, F. D. Gnanam, P. Ramasamy, *J. Mater. Sci. Lett.* **1988**, 7, 711–713.

[23] M. Sun, D. Z. Li, W. J. Li, Y. B. Chen, Z. X. Chen, Y. H. He, X. Z. Fu, *J. Phys. Chem. C* **2008**, *112*, 18076–18081.

[24] a) E. Cardenas, A. Arato, E. Perez-Tijerina, T. K. Das Roy, G. A. Castillo, B. Krishnan, *Sol. Energy Mater. Sol. Cells* **2009**, *93*, 33–36; b) B. Krishnan, A. Arato, E. Cardenas, T. K. Das Roy, G. A. Castillo, *Appl. Surf. Sci.* **2008**, *254*, 3200–3206; c) Y. Rodríguez-Lazcano, M. T. S. Nair, P. K. Nair, *J. Cryst. Growth* **2001**, *223*, 399–406; d) A. M. Salem, M. S. Selim, *J. Phys. D* **2001**, *34*, 12–17; e) C. D. Lokhande, B. R. Sankapal, R. S. Mane, H. M. Pathan, M. Muller, M. Giersig, V. Ganesan, *Appl. Surf. Sci.* **2002**, *193*, 1–10; f) M. T. S. Nair, Y. Pena, J. Campos, V. M. Garcia, P. K. Nair, *J. Electrochem. Soc.* **1998**, *145*, 2113–2120.

[25] a) N. Tigau, *Cryst. Res. Technol.* **2006**, *41*, 474–480; b) A. M. Farid, A. E. Bekheet, *Vaccum* **2000**, *59*, 932–939; c) F. Perales, F. Agullo-Rueda, J. Lamela, C. D. L. Heras, *J. Phys. D* **2008**, *41*, 045403/1–8.

[26] a) S. R. Gadakh, C. H. Bhosale, *Mater. Chem. Phys.* **2003**, *78*, 367–371; b) K. Y. Rajpure, C. H. Bhosale, *Mater. Chem. Phys.* **2002**, *73*, 6–12.

[27] a) G. Xie, Z. P. Qiao, M. H. Zeng, X. M. Chen, S. L. Gao, *Cryst. Growth Des.* **2004**, *4*, 513–516; b) M. S. Mo, Z. Y. Zhu, X. G. Yang, X. Y. Liu, S. Y. Zhang, J. Gao, Y. T. Qian, *J. Cryst. Growth* **2003**, *256*, 377–382; c) J. O. Ota, S. K. Srivastava, *Cryst. Growth Des.* **2007**, *7*, 343–347; d) Z. R. Geng, M. X. Wang, G. H. Yue, P. X. Yan, *J. Cryst. Growth* **2008**, *310*, 341–344.

[28] R. Malakooti, L. Cademartiri, A. Migliori, G. A. Ozin, *J. Mater. Chem.* **2008**, *18*, 66–69.

[29] J. Yang, Y. C. Liu, H. M. Lin, C. C. Chen, *Adv. Mater.* **2004**, *16*, 713–716.

[30] a) Y. Yu, R. H. Wang, Q. Chen, L. M. Peng, *J. Phys. Chem. B* **2006**, *110*, 13415–13419; b) Y. Yu, R. H. Wang, Q. Chen, L. M. Peng, *J. Phys. Chem. B* **2005**, *109*, 23312–23315.

[31] Q. F. Han, J. Lu, X. J. Yang, L. D. Lu, X. Wang, *Cryst. Growth Des.* **2008**, *8*, 395–398.

[32] G. Y. Chen, B. Deng, G. B. Cai, T. K. Zhang, W. F. Dong, W. X. Zhang, A. W. Xu, *J. Phys. Chem. C* **2008**, *112*, 672–679.

[33] Q. F. Lu, H. B. Zeng, Z. Y. Wang, X. L. Cao, L. D. Zhang, *Nanotechnology* **2006**, *17*, 2098–2104.

[34] M. S. Mo, Z. Y. Zhu, X. G. Yang, X. Y. Liu, S. Y. Zhang, J. Gao, Y. T. Qian, *J. Cryst. Growth* **2003**, *256*, 377–382.

[35] a) J. Tang, *Nano Lett.* **2006**, *6*, 2701–2706; b) Y. H. Hu, K. Z. Chen, *J. Cryst. Growth* **2007**, *308*, 185–188.

[36] J. H. He, M. Han, X. P. Shen, Z. Xu, *J. Cryst. Growth* **2008**, *310*, 4581–4586.

[37] A. T. Kelly, I. Rusakova, T. Ould-Ely, C. Hofmann, A. Luttge, K. H. Whitmire, *Nano Lett.* **2007**, *7*, 2920–2925.

[38] J. F. Banfield, S. A. Welch, H. Z. Zhang, T. T. Ebert, R. L. Penn, *Science* **2000**, *289*, 751–754.

[39] S. M. Lee, S. N. Cho, J. W. Cheon, *Adv. Mater.* **2003**, *15*, 441–444.

[40] V. P. Herzog, S. L. Harmer, H. W. Nesbitt, G. M. Bancroft, R. Flemming, A. R. Pratt, *Surf. Sci.* **2006**, *600*, 348–356.

[41] K. J. M. Bishop, C. E. Wilmer, S. Soh, B. A. Grzybowski, *Small* **2009**, *5*, 1600–1630.

[42] a) M. Meyer, A. Bée, D. Talbot, V. Cabuil, J. M. Boyer, B. Répetti, R. Garrigos, *J. Colloid Interface Sci.* **2004**, *277*, 309–315; b) F. C. Meldrum, S. T. Hyde, *J. Cryst. Growth* **2001**, *231*, 544–558; c) J. B. Liang, J. W. Liu, Q. Xie, S. Bai, W. C. Yu, Y. T. Qian, *J. Phys. Chem. B* **2005**, *109*, 9463–9483.

[43] S. King, K. Hyunh, R. Tannenbaum, *J. Phys. Chem. B* **2003**, *107*, 12097–12104.

[44] G. Machado, J. D. Scholten, T. D. Vargas, S. R. Teixeira, L. H. Ronchi, J. Dupont, *Int. J. Nanotechnol.* **2007**, *4*, 541–563.

[45] P. Migowski, J. Dupont, *Chem. Eur. J.* **2007**, *13*, 32–39.

[46] a) C. M. Park, Y. Hwa, N. E. Sung, H. J. Sohn, *J. Mater. Chem.* **2010**, *20*, 1097–1102; b) H. M. Yang, X. H. Su, A. D. Tang, *Mater. Res. Bull.* **2007**, *42*, 1357–1363.

[47] a) K. S. Choi, *Dalton Trans.* **2008**, 5432–5438; b) Z. G. An, J. J. Zhang, S. L. Pan, F. Yu, *J. Phys. Chem. C* **2009**, *113*, 8092–8096.

[48] a) L. Liu, H. J. Liu, H. Z. Kou, Y. Q. Wang, Z. Zhou, M. M. Ren, M. Ge, X. W. He, *Cryst. Growth Des.* **2009**, *9*, 113–117; b) H. Y. Zhou, S. L. Xiong, L. Z. Wei, B. J. Xi, Y. C. Zhu, Y. Q. Qian, *Cryst. Growth Des.* **2009**, *9*, 3862–3867.

[49] M. Hasan, I. V. Kozhevnikov, M. R. H. Siddiqui, A. Steiner, N. Winterton, *Inorg. Chem.* **1999**, *38*, 5637–5641.